Effect of polydispersity on the evolution of density fluctuations to lamellar crystals in linear polyethylene

Yvonne A. Akpalu[a] and Eric J. Amis
Polymers Division, National Institute of Standards and Technology, Gaithersburg, Maryland 20899

(Received 20 December 1999; accepted 6 April 2000)

The effect of polydispersity on structure development in linear polyethylenes is studied by simultaneous real time small-angle x-ray scattering (SAXS) and wide-angle x-ray scattering (WAXS). Our measurements show that below 128 °C, changes in the SAXS and WAXS intensity profiles for a broad molecular-weight distribution sample occur simultaneously as previously reported for a narrow molecular-weight distribution sample. We demonstrate that variations in the SAXS profile can be correlated with the morphological changes associated with the evolution of single chain folded crystal lamellae to lamellar aggregates. At 128 °C and higher temperatures, changes in the SAXS intensity profile for the broad molecular weight distribution sample occur much earlier than the onset of lamellar crystal growth evidenced in the WAXS profile. For the period before crystal growth is manifest in the WAXS scattering, the SAXS intensity at low angles increases while the domain size remains constant. The low-angle intensity uptake in SAXS can be best described by the Guinier approximation. On the other hand, the temperature dependence of the variation in the average crystal thickness during isothermal crystal growth is a function of the relative rates of primary crystallization and thickening at a given temperature. We discuss the effect of a broad distribution in chain length on the various stages in the development of the morphology. [S0021-9606(00)51025-3]

I. INTRODUCTION

he morphology obtained during crystallization of polyethylene is known to depend strongly on molecular weight[1] and polydispersity.[2–4] Such evidence has come primarily from studies employing static light scattering, microscopy, and differential scanning calorimetry. The level of crystallinity that can be obtained at a given temperature decreases as the molecular weight is increased.[5] However, the crystallization rate does not increase monotonically with molecular length, but rather a temperature-dependent maximum is observed (Fig. 1). This effect was originally recognized by Mandelkern *et al.*[2] In Fig. 1, the logarithm of the crystallization half-time (in min) is plotted against the logarithm of the viscosity-average molecular weight of molecular weight fractions of linear polyethylene. Fractions were obtained using elution column techniques from either unfractionated Marlex-50 or from a polymethylene sample prepared by the decomposition of diazomethane using boron ester catalysis.[6] The maximum crystallization rate (minimum in its inverse, $\tau_{1/2}$) is more pronounced at higher crystallization temperatures. The rate of the initial decrease in $\tau_{1/2}$ with increasing molecular weight is independent of crystallization temperature (Fig. 1). However, the rate of the subsequent increase in $\tau_{1/2}$ with chain lengths above that which corresponds to the maximum crystallization rate (minimum in $\tau_{1/2}$) depends on crystallization temperature. These results indicate that a slight dependence of the crystallization rate on chain length would occur at low crystallization temperatures ($\leqslant$125 °C) in the higher molecular weight range ($M_\eta \geqslant 10^5$). It is obvious from the above that broad molecular-weight distribution polymers are complex systems of chains exhibiting varying crystallization rates.

Despite the extensive research on polyethylene, there have been no systematic measurements by real-time small-angle x-ray scattering (SAXS) and wide-angle x-ray scattering (WAXS) of the effects of polydispersity on structural changes occurring during the crystallization process. Real time simultaneous SAXS and WAXS (Refs. 7–9) can be a useful tool for studying thermodynamic and kinetic factors affecting the morphological development of polymers. Variations in the crystal unit cell parameters and crystallinity can be determined from WAXS while the long period, lamellar thickness, interlayer amorphous thickness, and invariant can be determined from SAXS. By comparing the morphological quantities obtained from SAXS and WAXS to a model for the crystallizing system which accounts for changes in the fraction of lamellar aggregates, we have been able to separate primary and secondary crystallization and evaluate the relative importance of two secondary processes during and after primary crystallization of a narrow molecular-weight distribution linear polyethylene.[10] The two secondary processes are the formation of new lamellar stacks and increases in the crystallinity within lamellae. We have also shown[10] that for the narrow molecular weight distribution polymer studied, the observed changes in SAXS and WAXS scattering profiles can be divided into three distinctive stages which reflect the evolution of isolated crystals to lamellar aggregates as suggested by the microscopic observations of Toda.[11] A schematic of the three stages of mor-

[a]Address after July 2000: Department of Chemistry, Rensselaer Polytechnic Institute, Troy, NY 12180.

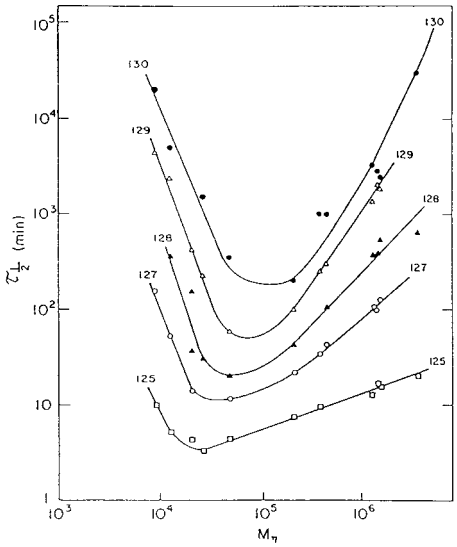

FIG. 1. Logarithm of crystallization half-time (in min) plotted against the logarithm of the viscocity-average molecular weight (M_η) for the five temperatures marked (from Ref. 2). Data was obtained for molecular weight fractions prepared from commercial polyethylenes.

phological development is shown in Fig. 2. From the microscopy studies, the authors were not able to determine if multilayered crystals develop immediately after the crystalline domains are formed. Our measurements show that there is a significant period where crystal growth can be attributed to monolayer crystals. During this period which we refer to as stage I, the fraction of crystals increases while the lamellar thickness remains constant. The subsequent development of lamellar stacks occurs in stage II. Stage II is characterized by a decrease in the periodicity of the sum of the crystalline and amorphous thicknesses, and the increasing dominance of the formation of lamellar stacks and increase in the crystallinity within lamellae over the growth of superstructures (primary crystallization). After the growth of the superstructures is complete (stage III), the crystallinity continues to increase further by increasing the fraction of lamellae and the thickening of existing lamellae. Primary crystallization occurs during stages I and II.

The objective of this paper is to study the effect of polydispersity on the nature of the density fluctuations during the period preceding lamellar crystal growth and the evolution of the fluctuations to lamellar crystals and supramolecular structures in linear polyethylene. Our measurements show that below 128 °C, changes in the SAXS and WAXS intensity profiles in the broad molecular-weight distribution sample ($M_w = 53\,070$ g/mol, $M_w/M_n = 2.9$) (Ref. 1) occur simultaneously as previously reported[10] for a narrow molecular-weight distribution sample ($M_w = 32\,100$ g/mol, $M_w/M_n = 1.1$).[1] For the broad molecular-weight distribution sample, we demonstrate that variations in the SAXS profile can be correlated to the morphological changes associated with the evolution of isolated crystals to lamellar aggregates as is the case for a narrow molecular-weight distribution sample. Above 128 °C, changes in SAXS and WAXS continue to occur simultaneously for the narrow molecular-weight distribution sample while for the broad molecular-weight distribution sample, changes in the SAXS intensity profile occur much earlier than the onset of lamellar crystal growth as evidenced in the WAXS profile. In contrast to other broad molecular-weight distribution polymers such as isotatic polypropylene[12] and poly(ethylene terephthalate)[13–15] where the variations in electron density fluctuations observed before crystal growth appear to obey spinodal-decomposition kinetics, the differences we see are consistent with what one would expect on the basis of the dependence of the crystallization rate on chain length and hence its distribution. The effect of a broad molecular weight distribution on the various stages in the development of the morphology is discussed.

II. EXPERIMENT

Measurements were performed on a narrow molecular-weight distribution sample (LPE1) and a broad molecular-

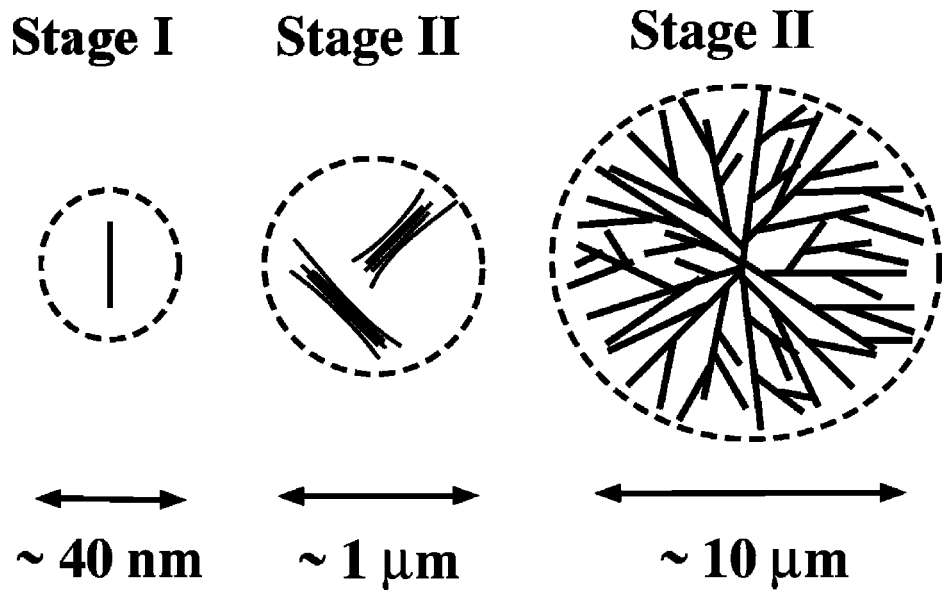

FIG. 2. Schematic drawings for the evolution of linear polyethylene spherulite.

TABLE I. Characterization data.

Sample code	Polymer	M_w (g/mol)	M_w/M_n
LPE1	SRM 1483	32 100 g/mol	1.1
LPE2	SRM 1475	53 070 g/mol	2.9

weight distribution sample (LPE2). LPE1 was prepared by a large-scale preparative gel permeation chromatography from a linear commercial polyethylene LPE2. The number average and weight average molecular weights[1] are given in Table I. A more detailed description of the characterization procedures used has been given in the NIST certificates of analysis for SRM 1483 (LPE1) and SRM 1475 (LPE2). The melting point of quenched samples of LPE1 and LPE2 is 130 °C. For comparative purposes, the theoretical equilibrium melting point of 145.5 °C (Ref. 16) will be used in describing the kinetics of both samples.

For x-ray measurements, samples were melt pressed in a vacuum laboratory hot press (Carver press, Model C) (Ref. 17) at 160 °C for 30 min at 13345 N. The molded films were then allowed to cool to room temperature under vacuum. A dual temperature chamber jump unit used for the melt crystallization experiments consists of two large thermal chambers maintained at the melt temperature [$T_1=160$ °C, (5–10) min] and a crystallization temperature (T_2). The copper sample cell was transferred rapidly (≈ 2 s) from one chamber (T_1) to the other (T_2) by means of a metal rod connected to a pneumatic device. A detailed description of the arrangement of the sample and of the two detectors used to measure WAXS and SAXS simultaneously has been provided previously.[18,19] Each polymer sample within the copper cell was 1.5 mm thick and 7 mm in diameter and was contained between two 25 μm thick Kapton films. The actual sample temperature during crystallization and melting was monitored by means of a thermocouple inserted into the sample cell. The crystallization temperatures studied (126 °C, 127 °C, 128 °C and 129 °C) were usually reached without overshooting, 120 s after transfer. Under isothermal conditions the fluctuations in the sample temperature are less than 0.2 °C. Unless stated otherwise, all references to time are times elapsed after transferring the sample to the crystallization chamber.

Time-resolved simultaneous SAXS/WAXS data were collected at the Advanced Polymer Beamline at Brookhaven National Laboratory, X27C. The radiation spectrum from the source was monochromated using a double multilayer monochromator and collimated with three 2° tapered tantalum pinholes to give an intense x-ray beam at $\lambda=1.307$ Å.[18] Two linear position sensitive detectors (European Molecular Biology Laboratory, EMBL) were used to collect the SAXS and WAXS data simultaneously. For SAXS, the detector was located 1940 mm from the sample position. A vacuum chamber was placed between the sample and both detectors to reduce air scattering and absorption. The usable span of scattering vector magnitudes [$q=(4\pi/\lambda)\sin(\theta)$ and 2θ is the scattering angle] for SAXS was in the range 0.01 Å$^{-1}<q<0.3$ Å^{-1} while that for WAXS was 0.5 Å$^{-1}<q<2.6$ Å^{-1}. Scattering patterns from silver behenate and Lupolen were used for angular calibration of the SAXS detector. NIST standards SRM 674A (α-Al_20_3) and SRM 675 (Mica), and Lupolen were used for angular calibration of the WAXS detector. A parallel plate ionizing detector placed before the sample cell was used to record the incident intensities. The experimental intensities were corrected for background scattering from the camera, temperature chamber and empty cell, incident intensity variations, and pixel-by-pixel detector sensitivity. The latter was established from the scattering of an Fe source. Two data acquisition times 15 s and 30 s were used depending on the crystallization rate.

III. DATA ANALYSIS

A detailed description of the methods used to obtain the integrated area under the amorphous peak intensity (I_{amorp}), the area under the crystalline reflections (I_{cryst}), the crystallinity from WAXS (w_c), the unit cell lattice parameters of a and b and the peak width of the crystalline and amorphous reflections have been given previously.[10] Several variables characterizing the lamellar morphology can be estimated from the one-dimensional correlation function [$\gamma_1(r)$] which is the Fourier transform of $I(q)q^2$,

$$\gamma_1(r)=\int_0^\infty I(q)q^2\cos(qr)dq/Q, \tag{1}$$

$$Q=\int_0^\infty I(q)q^2dq. \tag{2}$$

In order to obtain the invariant (Q) and $\gamma_1(r)$, the SAXS data were extrapolated to large q ($q=0.6$ Å^{-1}) wth the aid of a function representing the background scatter (I_B) and a modified Porod Law of the form,[20]

$$I(q)=\frac{K\exp(-\sigma^2q^2)}{q^4}+I_B. \tag{3}$$

Details of this procedure have been given previously.[21] Truncation of the data at $q=0.6$ Å^{-1} has been shown to give a reasonable approximation of correlation functions without excessive computational time.[21] Extrapolation to $q=0$ was performed by drawing a straight line from the origin to the first reliable data point at $q=0.01$ Å^{-1} in the $I(q)q^2$ plot.[22] For most purposes, the major contribution to the experimental invariant can be used to characterize structure development. Therefore we calculate a relative SAXS invariant (Q_{SAXS}) from the area under the $[I(q)-I_B]q^2$ vs q curve between the first reliable data point and 0.2 Å^{-1} beyond the value for which $[I(q)-I_B]q^2$ remains constant. Variations in Q_{SAXS} parallel Q and for consistency Q_{SAXS} is compared with the apparent crystallinity from WAXS (w_c). The crystallinity is referred to as ''apparent'' since corrections associated with crystalline disorder as discussed by Ruland[23,24] were not applied.

The long period which represents the sum of the crystalline and noncrystalline thicknesses can be estimated as the Bragg spacing corresponding to the peak position of the $I(q)q^2$ vs q curve (L_1). The Bragg spacing corresponding to the second SAXS peak is L_2. L_2 represents a distribution of periodicities upon a second-order reflection of the first SAXS

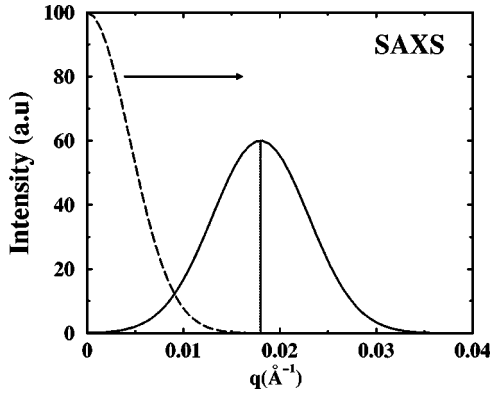

FIG. 3. Expected changes in the SAXS intensity profile during the evolution of isolated crystals to lamellar aggregates. Dashed line shows the intensity profile for isolated crystals while the solid line shows that corresponding to lamellar stacks. No changes in SAXS and WAXS will be observed before the formation of stable nuclei. Arrow shows the general progression in the peak maximum.

peak L_1.[10] In subsequent discussions we will refer to L_2 as the minor long period. In all figures, the standard deviation in the quantities estimated from SAXS and WAXS are plotted only when the uncertainty limits (standard deviation) are larger than the symbol size of plotted points.

IV. RESULTS AND DISCUSSION

A. Early stage crystal growth

In the classical view of polymer crystallization,[25] nucleation is initiated by large amplitude, local fluctuations of an order parameter, such as density, when a polymer solution or melt is cooled below it melting temperature. The result is the appearance of small nuclei of the stable crystalline phase and only those larger than a critical size grow. There is an induction period associated with the time to form the critical crystal nuclei from the amorphous state. The primary lamellar habit formed is a consequence of the anisotropic growth of the nuclei. The isolated crystalline domains formed will exhibit a monotonically decreasing profile with a maximum at $q=0$ (Fig. 3). In experiments, if a slope of 2 is obtained for a $\ln I$ vs q plot in the region where the data are fitted to this

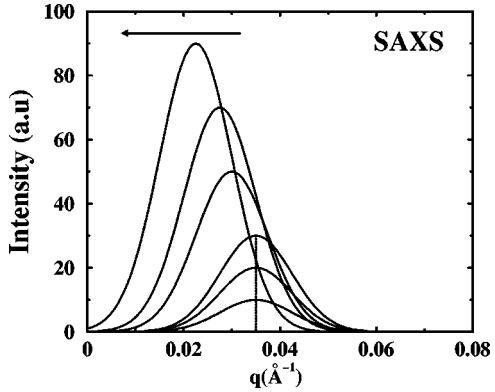

FIG. 4. Expected changes in the SAXS intensity profile for spinodal-assisted nucleation. Note that these changes occur when no Bragg peaks are evident in the WAXS intensity profile. Arrow shows the general progression in the peak maximum.

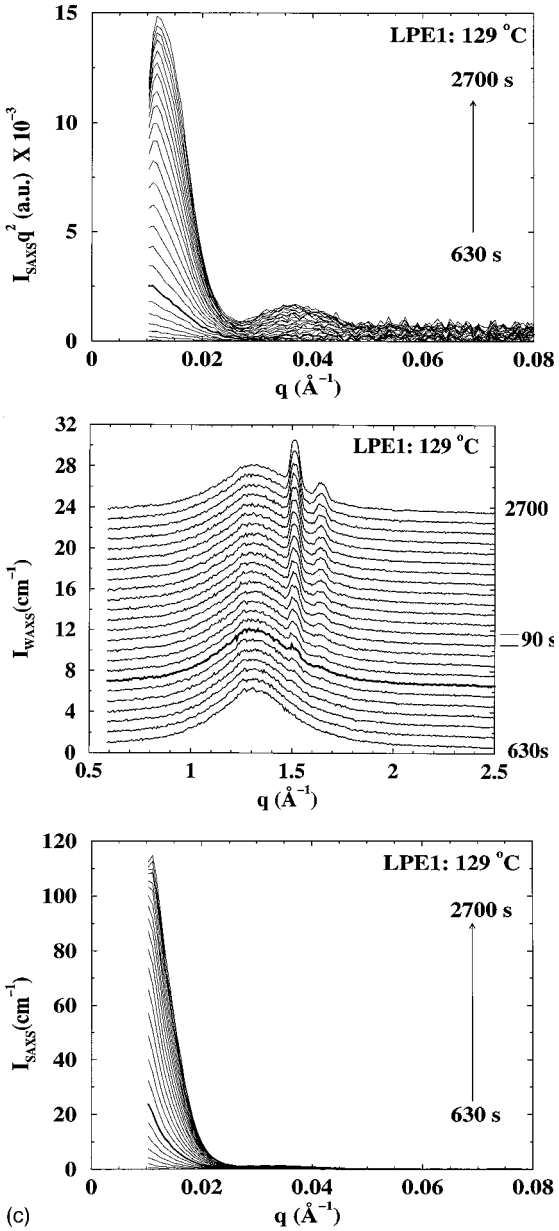

FIG. 5. Development of SAXS and WAXS during isothermal crystallization of LPE1 ($M_w=32\,100$, $M_w/M_n=1.1$) at 129 °C within the first 2700 s after melting at 160 °C for 5 min; (a) SAXS, intensity $I_{SAXS}q^2$; (b) WAXS, intensity I_{WAXS}; (c) SAXS, intensity I_{SAXS}. SAXS intensity represents excess scattering due to density fluctuations at the crystallization temperature since melt scattering has been subtracted. The relative standard deviation in the SAXS intensity values in the range 0.01 Å$^{-1}<q<0.02$ Å^{-1} is less than 2%. At higher wave vectors, the relative standard deviation increases with q and the maximum value is less than 15%. Bold curves denote the end of stage I. WAXS curves have been offset for clarity.

function, an appropriate functional form for the intensity profile is Guinier's Law.[26] The radius of gyration of the dense/crystalline domain can then be obtained. As lamellar aggregates develop, a peak at finite q corresponding to the periodicity of the repeat unit (one crystal plus one amorphous layer) will appear in the SAXS profile (Fig. 3). As the number of repeat units and the perfection in stacking increase, the relative intensity of the higher order maxima in the SAXS profile should increase. For this mechanism, no changes in the SAXS and WAXS profiles will be observed during the induction period.

In the case of a spinodal-assisted nucleation mechanism, recent experiments[12–15] report the development of a SAXS peak during the induction period. This feature has be attributed to the development of electron density fluctuations associated with partially ordered states. The scattering behavior preceding the formation and growth of stable crystal nuclei is consistent with the mechanism for spinodal decomposition (Fig. 4). Spinodal decomposition is a process involving the spontaneous growth of fluctuations. The characteristic length scale associated with the developing spinodal texture gives rise to a SAXS peak at finite q. During the early stages of growth, the amplitude of fluctuations increases exponentially with time while the peak position remains constant. As the domains coarsen, the peak position will shift to smaller wave vectors. Domain growth is arrested once Bragg peaks appear in the SAXS profile, signaling the formation of lamellar stacks.

Figures 5–7 show the change of the SAXS and WAXS intensity profiles during the early stage isothermal crystallization of LPE1 at 129 °C, LPE2 at 126 °C, and LPE2 at 129 °C after melting at 160 °C. The time dependence of the amorphous peak intensity, the integrated area under the crystalline peaks and the integrated SAXS intensity for each sample are shown in Figs. 8 and 9. At each temperature, even though the time dependence of the integrated intensities for both samples are similar, the onset of changes vary strongly with temperature. As a polymer melt is transformed to the crystalline state, one expects the peak intensity of the amorphous scattering to decrease while that of the crystalline reflections increases. As lamellar sheaves are developed, an increase in the SAXS peak intensity is expected. For LPE1, changes in SAXS and WAXS occur simultaneously when the sample is crystallized isothermally in the temperature range 127 °C to 130 °C (Fig. 8) while similar changes are observed for LPE2 below 128 °C (Fig. 9).

However, at 128 °C and 129 °C, the SAXS intensity at low wave vectors for LPE2 increases before any increase in the area under the crystalline reflections can be resolved in the WAXS scattering (Figs. 7 and 9). Similar results are also obtained at even higher temperatures. For both samples, the absence of a distinct peak in the SAXS profile may be due to a very small population of lamellar stacks and/or monolayer lamellar crystals. For LPE1, we have shown previously[10] that the SAXS intensity profiles during the initial stages of growth are characteristic of the growth of isolated crystals (Stage I). In addition, the intensity profiles during Stage I can be described by Guinier's Law for isolated domains at high dilution and for randomly oriented thin platelets. The intensity variations are given by[26]

$$I(q,t) \propto \exp\left[-\frac{R_g^2 q^2}{3}\right], \tag{4}$$

$$I(q,t) \propto q^{-2} \exp\left[-\frac{l_g^2 q^2}{12}\right], \tag{5}$$

where R_g is the radius of gyration of the isolated domain and l_g is the thickness of the platelet. Figures 8(a) and 9(a) show R_g as a function of time for LPE1 and LPE2 at 129 °C respectively. Typical Guinier plots using Eqs. (4) and (5) for both samples at 129 °C are shown in Figs. 10 and 11, respectively. At this temperature, a dense domain is formed initially when changes are observed in SAXS and the average size of this domain does not change. Similar results are obtained at lower temperatures when the initial stages can still be resolved (Table II). The average size of the domain obtained for LPE2 is about the same as that obtained for LPE1 at the same crystallization temperature (Table II).

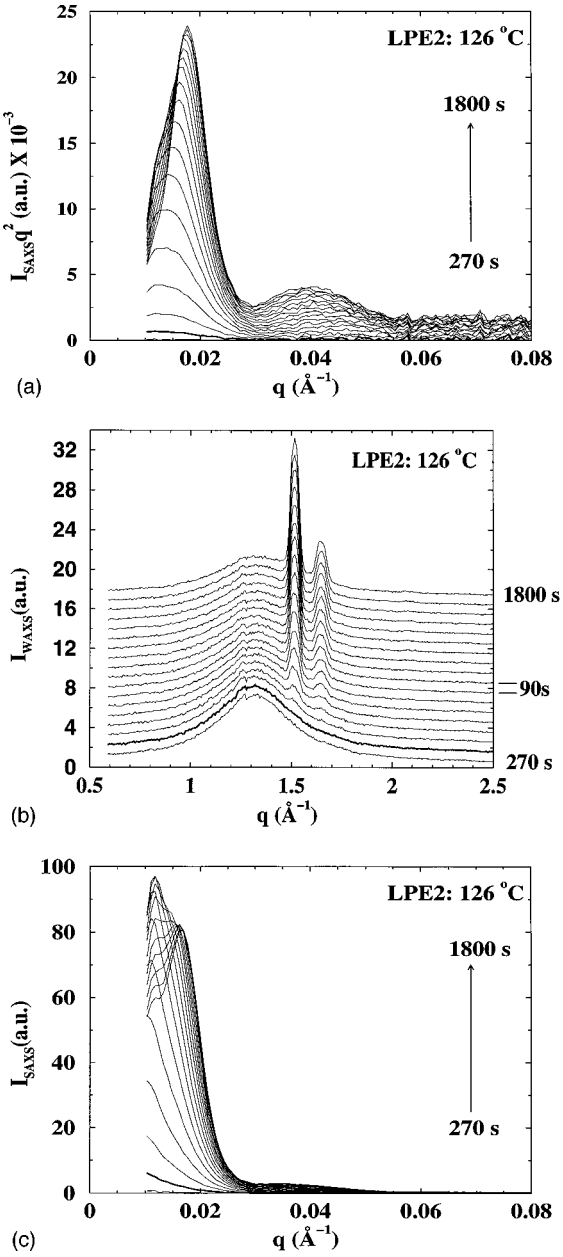

FIG. 6. Development of SAXS and WAXS during isothermal crystallization of LPE2 ($M_w = 53\,070$, $M_w/M_n = 2.9$) at 126 °C within the first 1800 s after melting at 160 °C for 5 min; (a) SAXS, intensity $I_{SAXS}q^2$; (b) WAXS, intensity I_{WAXS}; (c) SAXS, intensity I_{SAXS}. SAXS intensity represents excess scattering due to density fluctuations at the crystallization temperature since melt scattering has been subtracted. The relative standard deviation in the SAXS intensity values in the range 0.01 Å$^{-1} < q < 0.02$ Å^{-1} is less than 2%. At higher wave vectors, the relative standard deviation increases with q and the maximum value is less than 15%. Bold curves denote the end of stage I. WAXS curves have been offset for clarity.

The kinetic model of Hoffman *et al.*[25] predicts that the

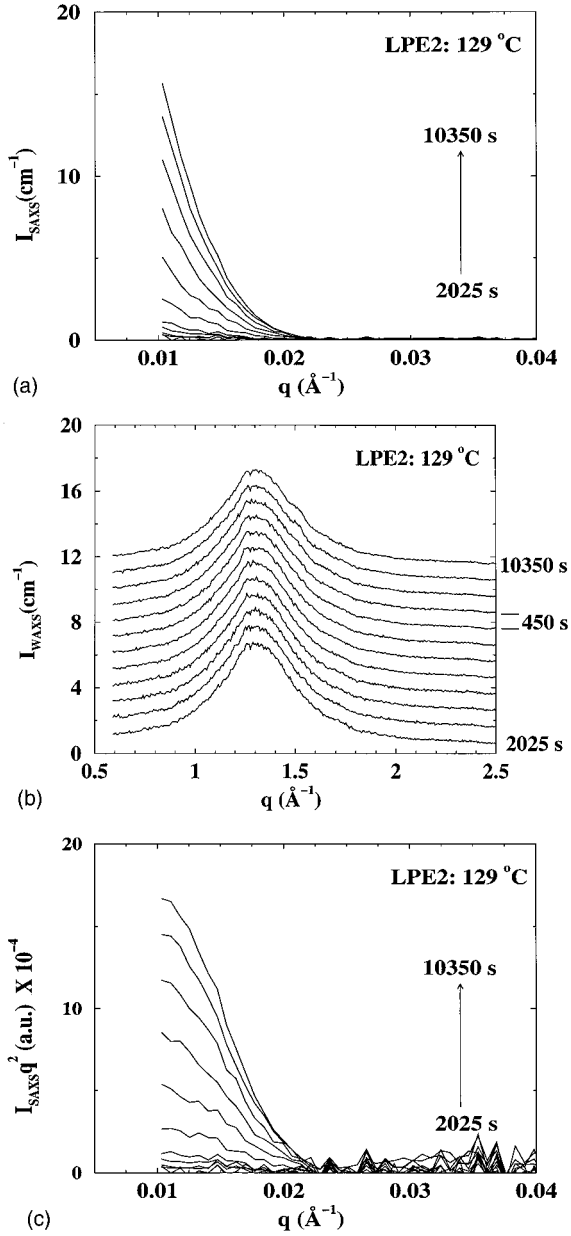

FIG. 7. Development of SAXS and WAXS during isothermal crystallization of LPE2 ($M_w=53\,070$, $M_w/M_n=2.9$) at 129 °C within the first 10 350 s after melting at 160 °C for 5 min; (a) SAXS, intensity I_{SAXS}; (b) WAXS, intensity I_{WAXS}; (c) SAXS, intensity $I_{SAXS}q^2$. SAXS intensity represents excess scattering due to density fluctuations at the crystallization temperature since melt scattering has been subtracted. The relative standard deviation in the SAXS intensity values in the range 0.01 Å$^{-1}<q<0.02$ Å^{-1} is less than 2%. At higher wave vectors, the relative standard deviation increases with q and the maximum value is less than 15%. Data shown is during stage I. WAXS curves have been offset for clarity.

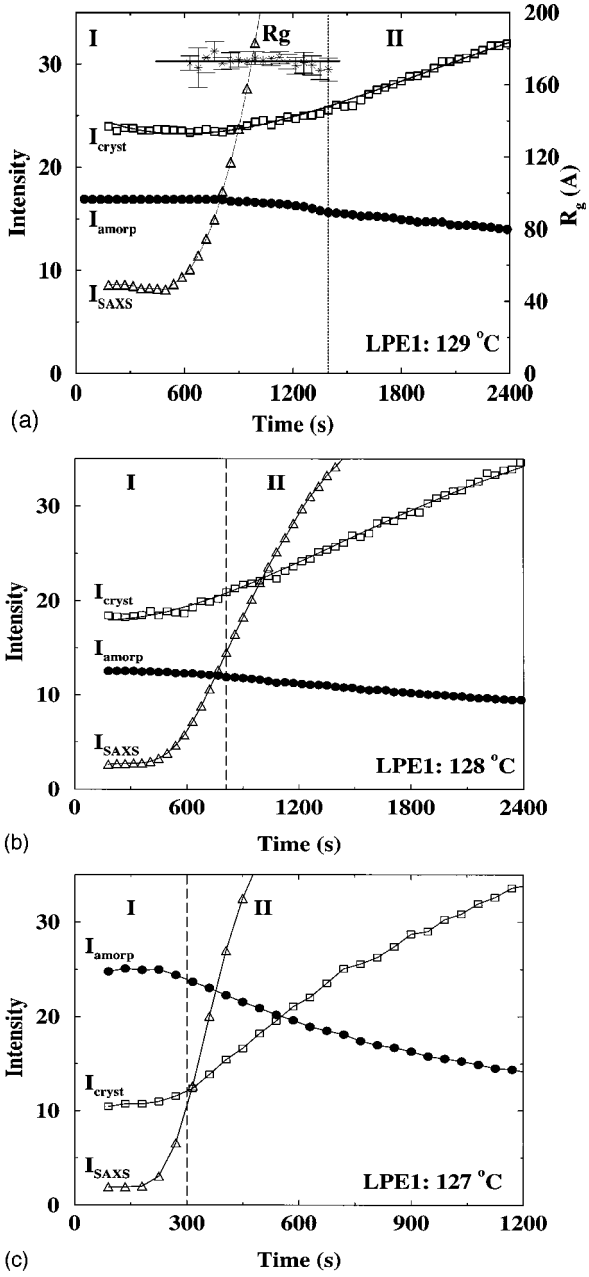

FIG. 8. Variation of integrated area under the crystalline reflections (I_{cryst}) in the WAXS profile, the amorphous peak intensity (I_{amorp}) and the integrated SAXS intensity (I_{SAXS}) during crystallization of LPE1 at (a) 129 °C; (b) 128 °C and (c) 127 °C. The radius of gyration (R_g) of the isolated domain during crystallization at 129 °C is shown in (a).

initial lamellar thickness formed (l^*) is given by

$$l^*=\frac{2\sigma_e T_m^0}{\Delta h_f \Delta T}+\delta l, \tag{6}$$

where the quantity Δh_f is the heat of fusion, the equilibrium melting point is T_m^0, $\Delta T=T_m^0-T_c$, σ_e is the interfacial free energy associated with the basal plane, and δl is the thickness increment above the minimum lamellar thickness which enables the secondary surface nucleus to enter a region of thermodynamic stability at the fastest rate at T_c.[25] The theory predicts a δl value of 10–15 Å. Experiments carried out on solution and on melt crystallized polyethylene under conditions where lamellar thickening is not observed, yield an average value $\delta l=43$ Å; $\delta l_{\min}=28.1$ Å and $\delta l_{\max}=58.7$ Å.[28] By substituting values appropriate to SRM 1483 crystallized from the melt[27] ($\Delta h_f=280\,J\,cm^{-3}$, $T_m^0=417$ K, and $\sigma_e=90\,mJ\,m^3$) and accounting for the variation in measured and predicted δl, l^* is found to range from 178 Å to 238 Å at 128 °C and 129 °C (Table II). The measured initial crystal thickness for LPE1 at 128 °C is 220 Å.[28] The Guinier plot, interpreted in terms of scattering by monolayer lamellar

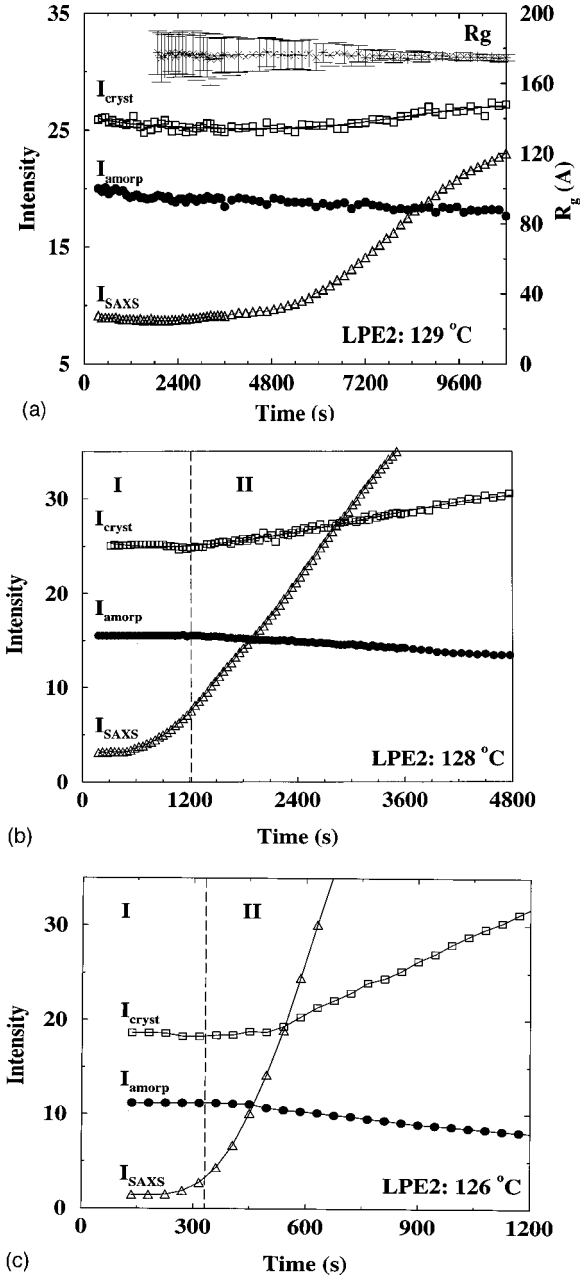

FIG. 9. Variation of integrated area under the crystalline reflections (I_{cryst}) in the WAXS profile, the amorphous peak intensity (I_{amorp}) and the integrated SAXS intensity (I_{SAXS}) during crystallization of LPE2 at (a) 129 °C; (b) 128 °C and (c) 126 °C. The radius of gyration (R_g) of the isolated domain during crystallization at 129 °C is shown in (a).

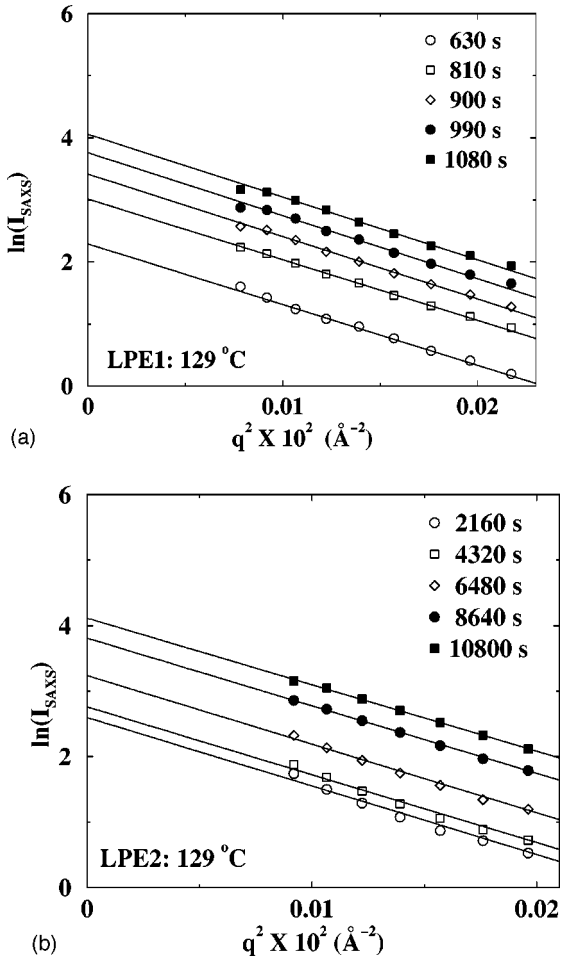

FIG. 10. Guinier plots for various crystallization times in stage I. (a) LPE1 at 129 °C; (b) LPE2 at 129 °C. Lines represent fits to the data points using Eq. (4).

crystals, should give a domain size similar to that found for the crystal thickness at the same temperature. The good agreement between the size of the platelet thickness obtained for LPE1 and LPE2 with the predicted initial lamellar thickness and that measured by Keller and Organ[28] suggests that the scattering during stage I can be attributed to isolated crystals (Table II). However, since the uncertainty in the domain size obtained with Eq. (4) is much smaller than that obtained for the platelet thickness by use of Eq. (5), we do not have platelets that can be described as infinitely wide such that one can assume that $l_g \ll b$, where the width of the platelet is denoted as b. The relatively good fit obtained by applying Eq. (5) indicates that $w > l_g$. Unfortunately, our current analysis does not allow us to determine the magnitude of w relative to l_g.[26]

The starting point for almost all analytical[31] and numerical[32] approaches to a theory of phase ordering (and separation) kinetics is a stochastic partial differential equation describing the evolution of an order parameter such as concentration or density. During the *early stages* of ordering after nucleating centers are formed, the amplitude of fluctuations reflected in the scattering intensity should increase exponentially with time while the characteristic domain size of the ordered phase should remain constant. If spinodal decomposition were to play a major role in the early stage crystallization process, the characteristic length scale associated with the developing spinodal texture should give rise to a SAXS peak at finite q which is inconsistent with the Guinier character of the SAXS intensity profile. Experimentally, the linear dependence of the logarithm of the scattered intensity at a given q with time for a range of q values is a strong indication of early stage ordering kinetics. During the induction period for LPE2 at 129 °C, the logarithm of SAXS intensity at low q increases linearly with time while the characteristic size of the dense domain remains *constant* (Fig. 12). This observation and the Guinier character of the SAXS

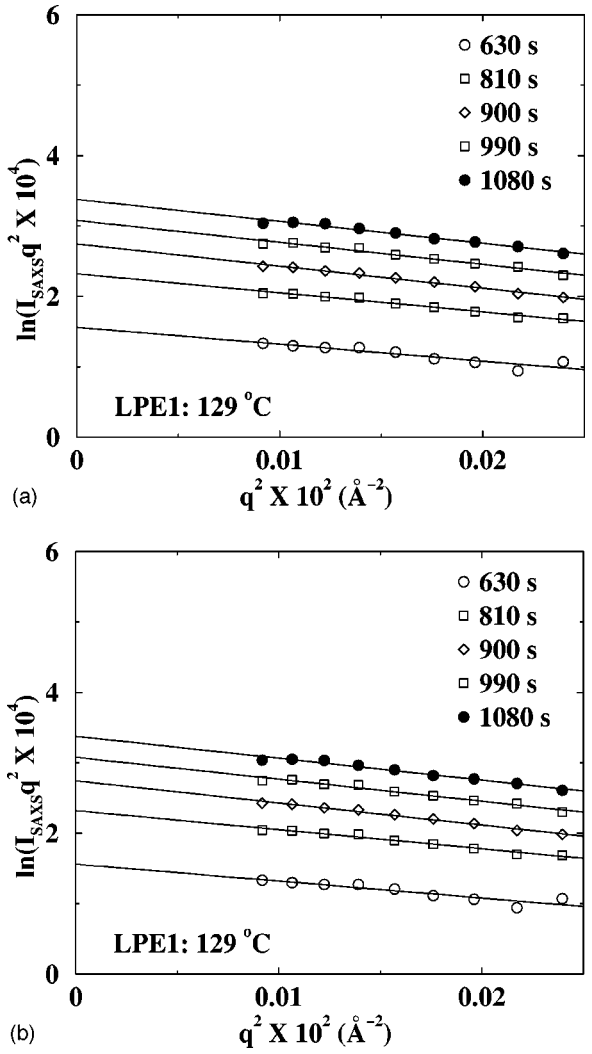

FIG. 11. Guinier plots for various crystallization times in stage I. (a) LPE1 at 129 °C; (b) LPE2 at 129 °C. Lines represent fits to the data points using Eq. (5).

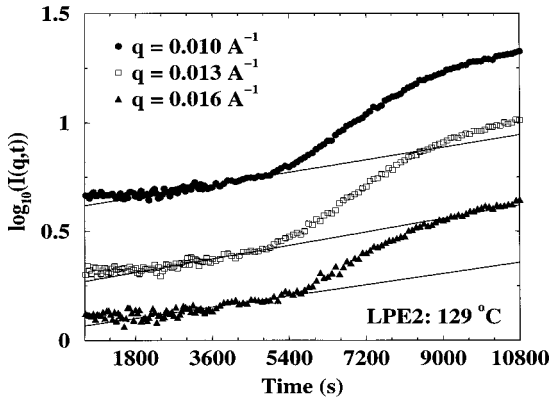

FIG. 12. Plot of $\log_{10}I(q)$ vs time at low q values during crystallization of LPE2 at 129 °C.

intensity profile indicate that fluctuations observed in the SAXS profile before crystal growth is manifest in WAXS, can be attributed to the local ordering of isolated domains.

In LPE2, the onset of crystal growth occurs much later than in LPE1 (Figs. 5–9). In Fig. 1, the decrease in the crystallization rate (longer $\tau_{1/2}$) with increasing molecular weight in the higher molecular weight range ($M_\eta \geqslant 10^5$) has been attributed to the increased viscosity of the medium and its effect on segmental mobility.[2] It follows that for a sample with a broad distribution in chain length, the environment for chains that can crystallize more rapidly can be very viscous. This increase in viscosity can slow down the nucleation kinetics and affect the quality of crystalline nuclei formed such that in LPE2 local crystalline order is not achieved initially and a gradual increase in the local order of the dense domain has to occur before the resulting crystal can grow. On the other hand, LPE1 is a sample with a narrower distribution in chain lengths hence the crystallization rate of each molecule should be similar. Our results can be interpreted to indicate that the local viscous environment may affect the nature of the crystal nuclei formed at a given temperature in addition to retarding the growth rate[25,27] of the crystals. These same effects should be observed for a narrow molecular weight distribution sample with a high molecular weight ($M_w \geqslant 10^5$).

During the period before crystal growth is manifest in the WAXS scattering, it is not clear whether the isolated domain obtained for LPE2 has sufficient order to be classified as crystal. The delayed appearance of changes in the WAXS intensity profile may be due to the initial formation of imperfect monolayer crystals, which do not give sufficient diffraction signals in WAXS but may exhibit enough density contrast from the amorphous phase in SAXS. If this is the case, the mechanism for the evolution of the density fluctuations before lamellar crystal growth is evident in WAXS may be as follows. It is only after a sufficient density value (ordering) in the dense phase has been attained that lamellar crystal growth becomes evident in SAXS and WAXS. The lamellar crystal growth process is characterized by a greater rate of increase in the SAXS intensity (Fig. 9) concurrent with an increase in the area under the crystalline reflections and with a decrease in the amorphous peak intensity (decrease in the concentration of amorphous regions). The enhancement of density fluctuations may also reflect improvements in the lateral stem packing of chains as the number of dense domains increases.

TABLE II. Domain sizes during stage I. Radius of gyration of isolated domains at high dilution (R_g); thickness of randomly oriented thin platelets (l_g); range of crystal thickness predicted by secondary nucleation (l^*). The l^* values reflect a range spanning the theoretical value of δl (10 Å) and the maximum value ($\delta l = 59$ Å) from previous studies (Ref. 28) on LPE1. The $\pm$ values denote the standard deviation and T denotes temperature.

Sample	T(°C)	R_g (Å)	l_g (Å)	l^* (Å)
LPE1	128	(171±7) Å	(169±22) Å	178 Å–227 Å
LPE1	129	(173±5) Å	(194±14) Å	189 Å–238 Å
LPE2	128	(172±8) Å	(195±15) Å	178 Å–227 Å
LPE2	129	(174±8) Å	(197±16) Å	189 Å–238 Å

B. Evolution of lamellar aggregates

For LPE1 and LPE2, superstructures such as spherulites and axialites consisting of crystalline and noncrystalline re-

gions grow during crystallization from the melt.[25,29,11] The SAXS invariant for a system where all the crystallizable units are within supermolecular structures is given by[30]

$$Q_{\mathrm{SAXS}} = C x_s x_L x_{CL}(1-x_{CL})(\Delta\rho)^2. \tag{7}$$

In Eq. (7), C is a factor dependent on geometry and other quantities that are kept constant during the experiment, $\Delta\rho$ is the electron density difference between the crystalline and amorphous phases, x_s is the volume fraction of polymer transformed into supermolecular structure, x_L is the volume fraction of lamellar stacks within the superstructures, and x_{CL} is the fraction of crystals within the lamellar stacks. The volume fraction of lamellar stacks is given by $x_s x_L$. The implicit assumption of this model is that all the crystals are in lamellar stacks and there are only two phases (crystalline and amorphous). In addition, the fraction $1-x_s$, which is not involved in forming the supermolecular structures, does not contribute to Q_{SAXS}.[30]

The crystallinity index measured by WAXS (w_c) is the total mass fraction of crystals within the sample that is related to the above quantities by

$$w_c = \left(\frac{\rho_c}{\rho_s}\right)\Phi_c, \tag{8}$$

$$\Phi_c = x_s x_L x_{CL}, \tag{9}$$

$$\rho_s = \rho_c \Phi_c + \rho_a(1-\Phi_c), \tag{10}$$

where Φ_c is the volume fraction crystallinity that can be estimated from WAXS. The electron densities of the crystalline and amorphous regions are designated by ρ_c and ρ_a and that of the sample is ρ_s. The factor (ρ_c/ρ_s) is included to convert volume fractions to mass fractions.

According to this model, x_s increases from 0 to 1 during the growth of superstructures (primary crystallization). During the primary crystallization (stages I and II) of most polymers, the change of x_{CL} is small as compared to the variation in the fraction of lamellae within the superstructures ($x_s x_L$) so that x_{CL} can be considered to be almost constant (Fig. 2). As a result, Q_{SAXS} and w_c or Φ_c are correspondingly proportional to $x_s x_L$ [Eqs. (7) and (8)]. This will also be the case if spherulitic growth occurs rapidly and the fraction of lamellar stacks within the spherulite continues to increase while x_{CL} remains constant. In contrast, during secondary crystallization involving only an increase in x_{CL} with x_L and x_s constant, Q_{SAXS} is proportional to $x_{CL}(1-x_{CL})$ while w_c is proportional to x_{CL}. Thus, for this model during secondary crystallization, the change in w_c will be larger than the change of Q_{SAXS}, in contrast to primary crystallization when Q_{SAXS} and w_c are proportional to each other. If the sample is completely filled with lamellar stacks $w_c = x_{CL}$.

In stage I, the relative invariant (Q_{SAXS}) and crystallinity (w_c) increase in proportion as the fraction of material within the superstructures increases with x_{CL} relatively constant (Fig. 13). The scattering during this stage is characteristic of individual lamellae and can be interpreted in terms of a skeletal spherulite model, wherein the lamellar ribbons extend as units or as complete groups outward into the melt.[33,34] Although the superstructures continue to grow in stage II, increases in the fraction of lamellar stacks (x_L) continue to dominate over any increases in the crystallinity within lamellae (increases in x_{CL}).

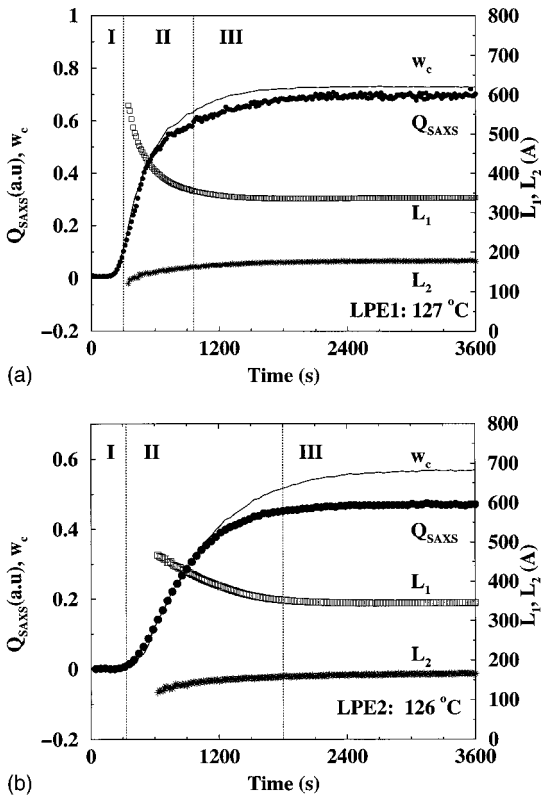

FIG. 13. Changes in morphological quantities for synchrotron SAXS/WAXS during crystallization of (a) LPE1 at 127 °C, and (b) LPE2 at 126 °C; degree of crystallinity determined from WAXS w_c (—), SAXS invariant Q (●), the long period (L_1), and the minor long period (L_2) obtained from the Iq^2 curve.

The shift in the first maximum of the correlation function to smaller spacings, and the increase in the intensity of the second order maximum with crystallization time, is consistent with the development of lamellar stacks with a high level of periodicity in stacking during primary crystallization of LPE1 (Fig. 14). A two-phase analysis of the correlation function of SAXS data yields estimates for the long period

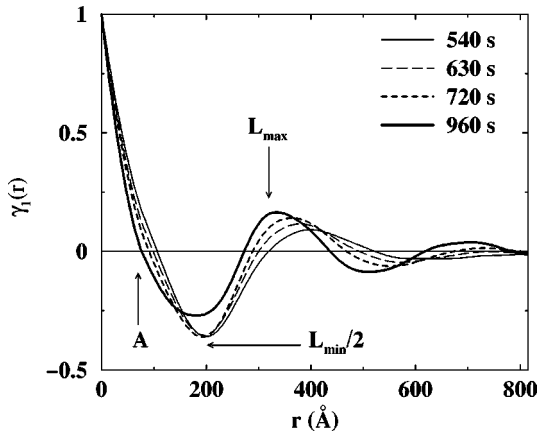

FIG. 14. Correlation functions calculated from the time-resolved SAXS profiles of LPE1 at 127 °C. Profiles during stage II are shown.

TABLE III. Limiting values morphological parameters. Period of the first SAXS peak (L_1^*); period of the second SAXS peak (L_2^*); first maximum in the correlation function ($L_{\max}^*$); twice the first minimum in the correlation function ($L_{\min}^*$); thickness of the thicker phase (l_1^*); thickness of the thinner phase (l_2^*); crystallinity from WAXS w_c^*. The * denotes that the values shown are for $t=7200$ s. T denotes temperature. The standard deviation in L_1^*, L_2^*, $L_{\max}^*$, and $L_{\min}^*$ is about 1 Å while that for l_1^* and l_2^* is about 5 Å.

Sample	T(°C)	L_1^* (Å)	L_2^* (Å)	$L_{\min}^*$ (Å)	$L_{\max}^*$ (Å)	l_1^* (Å)	l_2^* (Å)	w_c^*
LPE1	127	343 Å	180 Å	288 Å	337 Å	242 Å	95 Å	0.73
LPE1	128	373 Å	180 Å	392 Å	360 Å	246 Å	114 Å	0.53
LPE1	129	454 Å	185 Å	462 Å	417 Å	262 Å	155 Å	0.43
LPE2	126	351 Å	169 Å	352 Å	338 Å	229 Å	109 Å	0.58
LPE2	128	478 Å	170 Å	458 Å	431 Å	288 Å	143 Å	0.19

and thickness of both crystalline and amorphous phases.[30,35,36] We have previously stated that the long period can be estimated from the Bragg spacing corresponding to the peak position of $I(q)q^2$ vs q curve. The long period can also be estimated as the position of the first maximum in the correlation function ($L_{\max}$) and twice the position of first minimum in the correlation function ($L_{\min}$) (Fig. 14). $L_{\max}$ represents the most probable distance between two crystals separated by an amorphous layer while $L_{\min}$ represents the most probable distance between crystal-amorphous interfaces. For an ideal two phase model, $L_1=L_{\max}=L_{\min}$. For most polymers, the distribution in the crystal and amorphous thicknesses are not the same and are usually broad, which results in $L_1\neq L_{\max}\neq L_{\min}$.[30]

Several methods have been outlined for estimating the crystalline and amorphous thicknesses from a two-phase analysis of the correlation function.[30,35,36] The method that we have employed[30] is summarized by the simple expression

$$A=x_1(1-x_1)L_{\max}, \tag{11}$$

where x_1 is defined by

$$l_1=x_1L_{\max} \quad \text{and} \quad l_2=(1-x_1)L_{\max}. \tag{12}$$

In Eq. (11), A is the first intercept of the correlation function with the r axis (Fig. 14) and $L_{\max}$ is the long period corresponding to the first maximum of the correlation function. Note that Eq. (11) is quadratic in x_1 and can be solved to obtain two solutions whose sum equals 1. We choose the larger value of x_1 and as a result l_1 represents the thicker phase and the smaller phase is l_2.[30,37,38] It follows that if l_1 is the thickness of the crystalline phase then $x_1=x_{CL}$. Care should be taken when using the morphological quantities l_1 and l_2 for subsequent analysis since the thickness distribution of each phase is not accounted for. However, the trends in both phases are captured by variations in l_1 and l_2. In order to assign the two calculated thicknesses l_1 and l_2 to the crystal and interlayer amorphous thickness additional information from WAXS is required. In stage III where x_s is constant, the assignment of l_2 as the crystalline phase requires that the volume of lamellar stacks is greater than 1 ($x_sx_L>1$) while for mass balance of the crystal phase the following condition $x_sx_L\leqslant 1$ must be satisfied. Thus in order to fulfill the criterion of mass balance for the crystalline phase, l_1 must be crystalline and the smaller l_2 must be the noncrystalline layer. Moreover our values for the crystalline (l_1) and amorphous thickness (l_2) at long times (Table III) are in good agreement with reported[39] values ($l_1=245$ Å–265 Å) and ($l_2=90$ Å–130 Å) obtained for LPE1 annealed in the temperature range we studied (126 °C–130 °C) in the range of chain lengths that can crystallize with decreasing temperature.

At all temperatures, the variation in $L_{\max}$ parallels L_1 (Figs. 12, 15, and 16) but $L_{\max}$ is slightly less than L_1 (Table III). At long times, $L_{\min}>L_{\max}>L_1$ for LPE1 at $T_c>127$ °C and for LPE2 above 125 °C. The physical implication of this observation is that the variance of the thinner phase (amorphous) is much larger than that of the thicker phase (crystalline).[30] At lower temperatures this inequality is reversed and there is a relatively larger variation in the crystalline phase than the amorphous phase (Table III). This reversal is consistent with a broadening in the distribution of lamellar thicknesses as the range of chain lengths that can crystallize increases with decreasing temperature.

The long period (L_1) for LPE2 is much larger than that for LPE1 while the minor long periods (L_2) differ by about 10 Å at the same temperature (Table III). A detailed analysis of our synchrotron WAXS data shows that the a and b unit cell lattice parameters for both samples are identical, suggesting that polydispersity does not affect the crystal lattice (Table IV). The full-width at half-maximum also remains constant (Table IV) as the molecular weight distribution increases from LPE1 to LPE2, suggesting that the perfection of the crystals and the lateral packing of stems does not change. As a consequence, the differences between the major long periods for LPE1 and LPE2 must result from variations in their amorphous content.

As temperature is increased, the variations in the morphological parameters extracted from the correlation function during crystallization are less pronounced (Figs. 15 and 16). At temperatures below 129 °C for LPE1 [Figs. 15(a) and 15(b)] and below 128 °C for LPE2 [Fig. 16(b)] l_1 decreases initially and l_2 remains relatively constant when the crystallinity from WAXS is less than 0.5. If l_1 is the average crystal thickness then it is likely that the sharp initial decrease in l_1 while l_2 is constant is consistent with the formation of new crystals (increase in x_L) at a rate for which the thickening of existing lamellae (increase in x_{CL}) is negligible in comparison. The new crystals are probably formed by nucleation on pre-existing crystals or from a melt restrained by lamellae formed at earlier times. The subsequent increase in l_1 and decrease in l_2 can be attributed to increases in the crystallin-

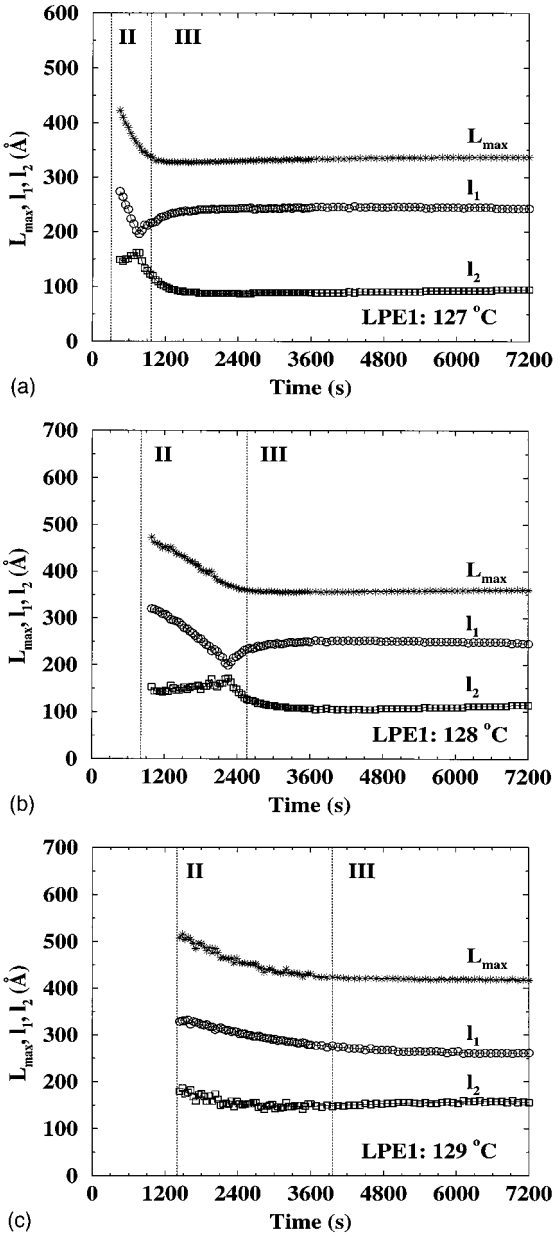

FIG. 15. Estimated values of long period $L_{\max}$, thicker phase (l_1) and thinner phase (l_2) during crystallization of LPE1 at (a) 127 °C; (b) 128 °C; (c) 129 °C.

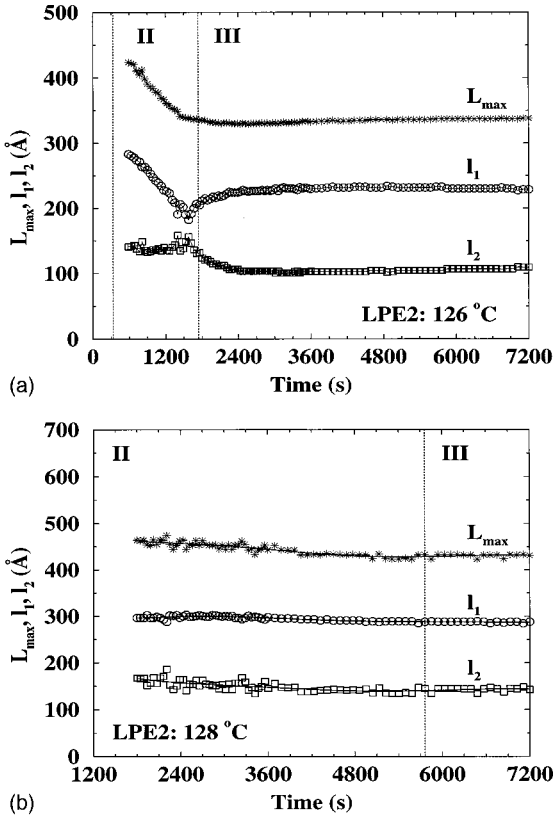

FIG. 16. Estimated values of long period $L_{\max}$, thicker phase (l_1) and thinner phase (l_2) during crystallization of LPE2 at (a) 126 °C; (b) 128 °C.

ity within the lamellar stacks by conversion of the interlayer amorphous material. Here the increase in x_{CL} dominates changes in x_L. As expected, the interlayer amorphous thickness in LPE2 is much larger than that in LPE1 at a given temperature (Table III).

At higher temperatures [Figs. 15(c) and 16(b)], the slight decrease in l_1 indicates a smaller range in the crystal thickness of the later forming crystals. After this initial decrease no subsequent increase is observed. The reason for this may be that at higher temperatures the growth rate of the superstructure formed may be slow enough to allow the addition of a chain fold and possible reorganization of the stem at the growth front resulting in improvements in the stem packing before another molecule is added. The slower variation of $L_{\max}$, l_1 and l_2 at higher temperature may also indicate a narrowing in the distribution of crystallizing chains and hence a narrower range of growth rates with increasing temperature. This narrowing is consistent with the decrease in the number of stacks formed with increasing temperature. Such a decrease is suggested by the variation of the limiting crystallinity (w_c^*) with temperature for LPE1 and LPE2 (Table III). At long times, $x_s \approx 1$ and below 129 °C, $x_{CL} \approx 0.7$, where $x_{CL} = l_1^*/L_{\max}^*$. Thus the decrease in w_c^* with increasing temperature is consistent with a large decrease in the fraction of stacks x_L as fewer chains crystallize. The slightly lower value of x_{CL} (0.63) for LPE1 at 129 °C is consistent with the much larger amorphous thickness at this temperature (Table III). Since similar trends in $L_{\max}$, l_1 and l_2 are observed for LPE1 and LPE2 with increasing temperature, the variation of these parameters must depend primarily on the relative rates of primary crystallization and thickening which in turn are strongly temperature dependent. Our results suggest that in the limit of $M_w/M_n = 1$ and high crystallization temperatures ($T_c > 128$ °C), crystal growth should occur at constant crystal thickness.[40]

V. CONCLUSIONS

The simultaneous measurement of SAXS and WAXS for narrow and broad molecular weight distribution polyethylene demonstrates that the differences observed during the development of the morphology can be attributed to the dependence of the crystallization rate on chain length and polydispersity. Broadening of chain length distribution slows down the rate at which the morphological variables derived from

TABLE IV. Average values of the a and b unit cell lattice parameters, full-width at half-maximum (Γ) of the (110) and (200) crystalline reflections during crystallization of LPE1 and LPE2 at various crystallization temperatures (T_c). Average values are for times greater than 3600 s. The $\pm$ values denote the standard deviation.

Sample	T_c (°C)	a (Å)	b (Å)	Γ_{110} (Å)	Γ_{200} (Å)
LPE1	127	(7.634±0.002) Å	(4.937±0.002) Å	(0.045±0.002) Å	(0.053±0.007) Å
LPE1	128	(7.644±0.003) Å	(4.945±0.002) Å	(0.048±0.004) Å	(0.056±0.007) Å
LPE1	129	(7.640±0.004) Å	(4.945±0.002) Å	(0.048±0.005) Å	(0.055±0.007) Å
LPE2	126	(7.625±0.005) Å	(4.938±0.002) Å	(0.044±0.002) Å	(0.052±0.001) Å
LPE2	128	(7.620±0.004) Å	(4.950±0.002) Å	(0.042±0.001) Å	(0.057±0.002) Å

SAXS and WAXS vary due to the dilution of the chain lengths that can crystallize more readily and affects the local crystalline order of the crystal nuclei. The interlayer amorphous thickness increases with polydispersity and temperature as the concentration of slower growing chains increases. In contrast, the temperature dependence of the variation in the average crystal thickness derived from SAXS is determined by the relative rates of primary crystallization and lateral readjustments (thickening) at a given temperature.

ACKNOWLEDGMENTS

SAXS and WAXS were carried out at the Advanced Polymer Beamline, constructed by Professors Benjamin Hsiao and Benjamin Chu, at the National Synchrotron Light Source, Brookhaven National Laboratory. We would like to thank Feng-ji Yeh and Dr. Lizhi Liu for help with the synchrotron x-ray setup. We would also like to thank Dr. Charles M. Guttman for providing the polymers studied and Dr. Freddy Khoury for his many helpful suggestions and discussions. We acknowledge helpful discussions with Dr. Charles Han, Dr. Jack Douglas, and Dr. Boualem Hammouda.

[1] According to ISO 31-8, the term ''Molecular Weight'' has been replaced by ''Relative Molecular Mass,'' with the symbol M_r. Thus, if this nomenclature and notation were to be followed in this publication, one would write $M_{r,n}$ instead of the historically conventional M_n for the number average molecular weight, with similar changes for M_w and it would be called the ''Number Average Relative Molecular Mass.'' The conventional notation, rather than the ISO notation, has been employed for this publication.
[2] L. Mandelkern, J. G. Fatou, and K. Ohno, J. Polym. Sci., Polym. Lett. Ed. **6**, 615 (1968).
[3] J. Maxfield and L. Mandelkern, Macromolecules **10**, 1191 (1977).
[4] I. G. Voigt-Martin, E. W. Fischer, and L. Mandelkern, J. Polym. Sci., Polym. Phys. Ed. **18**, 2347 (1980).
[5] L. Mandelkern, Acc. Chem. Res. **23**, 380 (1990).
[6] J. G. Fatou and L. Mandelkern, J. Phys. Chem. **69**, 417 (1965).
[7] M. Bark, H. G. Zachmann, R. Alamo, and L. Mandelkern, Makromol. Chem. **193**, 2363 (1992).
[8] H. H. Song, R. S. Stein, Q. D. Wu, M. Ree, J. C. Phillips, A. LeGrand, and B. Chu, Macromolecules **21**, 1180 (1988).
[9] H. H. Song, Q. D. Wu, B. Chu, M. Satkowski, M. Ree, R. S. Stein, and J. C. Phillips, Macromolecules **23**, 2380 (1990).
[10] Y. A. Akpalu and E. J. Amis, J. Chem. Phys. **111**, 8686 (1999).
[11] A. Toda, Colloid Polym. Sci. **270**, 667 (1992).
[12] N. J. Terrill, P. A. Fairclough, E. Towns-Andrews, B. U. Koanschek, R. J. Young, and A. J. Ryan, Polymer **39**, 2381 (1998).
[13] M. Imai, K. Kaji, and T. Kanaya, Phys. Rev. Lett. **71**, 4162 (1993).
[14] M. Imai, K. Mori, T. Mizukami, K. Kaji, and T. Kanaya, Polymer **33**, 4451 (1992).
[15] M. Imai, K. Kaji, and T. Kanaya, Macromolecules **27**, 7103 (1994).
[16] P. J. Flory and A. J. Vrij, J. Am. Chem. Soc. **85**, 3548 (1963).
[17] Certain equipment and instruments or materials are identified in the paper in order to adequately specify the experimental details. Such identification does not imply recommendation by the National Institute of Standards and Technology, nor does it imply the materials are necessarily the best available for the purpose.
[18] B. S. Hsiao, B. Chu, and F. Yeh, NSLS Newsletter, July 1 (1997).
[19] B. S. Hsiao, K. H. Gardner, D. Q. Wu, and B. Chu, Polymer **34**, 3996 (1993).
[20] J. J. Koberstein, B. Morra, and R. S. Stein, J. Appl. Crystallogr. **13**, 34 (1980).
[21] A. J. Ryan, J. L. Stanford, W. Bras, and T. M. W. Nye, Polymer **38**, 759 (1997).
[22] T. Russell, in *Handbook on Synchrotron Radiation*, edited by G. Brown and D. E. Moncton (Elsevier Science, New York, 1991), Vol. 3, Chap. 11, pp. 379–469.
[23] W. Ruland, Acta Crystallogr. **14**, 1180 (1961).
[24] W. Ruland, Polymer **5**, 80 (1964); **220**, 19 (1964).
[25] J. D. Hoffman, G. T. Davis, and J. I. Lauritzen, in *Treatise on Solid State Chemistry*, edited by N. B. Hannay (Plenum, New York, 1976), Vol. 3, Chap. 7.
[26] A. Guinier and G. Fournet, *Small-Angle Scattering of X Rays* (Wiley, London, 1955).
[27] J. D. Hoffman, Polymer **23**, 656 (1982).
[28] S. J. Organ and A. Keller, J. Mater. Sci. **20**, 1616 (1985).
[29] J. D. Hoffman, L. J. Frolen, G. S. Ross, and J. I. Lauritzen, Jr., J. Res. Natl. Bur. Stand., Sect. A **79**, 671 (1975).
[30] C. Santa Cruz, N. Stribeck, H. G. Zachmann, and F. J. Balta-Calleja, Macromolecules **24**, 5980 (1991).
[31] For a review, see J. D. Gunton, M. San Miguel, and P. S. Saint, in *Phase Transitions and Critical Phenomena*, edited by C. Domb and J. L. Lebowitz (Academic, New York, 1983), Vol. 8.
[32] For a review, S. Puri and Y. Oono, Phys. Rev. A **38**, 1542 (1988).
[33] J. M. Shultz, J. S. Lin, and R. W. Hendricks, J. Appl. Crystallogr. **11**, 551 (1978).
[34] J. M. Shultz, J. Polym. Sci., Polym. Phys. Ed. **14**, 2291 (1976).
[35] G. R. Strobl and M. Schneider, J. Polym. Sci., Polym. Phys. Ed. **18**, 1343 (1980).
[36] C. G. Vonk and A. P. Pijpers, J. Polym. Sci., Polym. Phys. Ed. **23**, 2517 (1985).
[37] R. Verma, H. Marand, and B. Hsiao, Macromolecules **29**, 7767 (1996).
[38] H. Marand, V. Velikov, R. K. Verma, P. M. Cham, V. Prabu, and D. Dillard, Polym. Prepr. (Am. Chem. Soc. Div. Polym. Chem.) **36**, 263 (1995).
[39] M. Peeters, N. Goderis, H. Reynaers, and V. Mathot, J. Polym. Sci., Polym. Phys. Ed. **37**, 83 (1999).
[40] L. Mandelkern, R. G. Alamo, and M. A. Kennedy, Macromolecules **23**, 4721 (1990).